Aquatic Ecology **37:** 307–324, 2003.

The 3D physical-biological model study in the Egyptian Mediterranean coastal sea

Waleed Hamza[1,4,*], Peeter Ennet[2], Rein Tamsalu[2] and Vladimir Zalesny[3]
*[1]Department of Environmental Sciences, Faculty of Science, Alexandria University, Alex, 21511, Egypt; [2]Estonian Marine Institute, Paldiski Str. 1, Tallinn, Estonia; [3]Institute of Numerical Mathematics, Russian Academy of Sciences (RAS), Moscow, Russia; [4]Current address: Biology Dept., Faculty of sciences, United Arab Emirates University, P.O. Box 17551, Al-Ain, U.A.E.; *Author for correspondence (e-mail: w.hamza@uaeu.ac.ae; fax: +971-3-767-1291)*

Received 15 August 2002; accepted in revised form 15 August 2002

Key words: Coastal ecosystem, Management, Numerical modelling, River Nile, Sewage discharge, Zooming

Abstract

The ecosystem of the Egyptian Mediterranean coastal area between longitudes 29°45′ E and 33°45′ E was seasonally investigated. The obtained data sets for a variety of environmental variables were previously interpolated over the studied area, and used in the coupled physical-biological model Fin-Est. Here, the model has been implemented to solve the central problems in case of modeling local areas and the handling of open boundaries and initial conditions, which almost have significant influence on the results, of both the hydrodynamic and the ecosystem models calculation. In the present study, a multi-step calculations procedure was used in applying the 3 D coupled model at first for the entire Egyptian Mediterranean coastal area. Then, it runs for local areas obtaining the initial conditions and the open boundary ones from larger area calculations. In particular, the zoom-in approach was used for the detailed study of the Eastern Harbour of Alexandria city-Egypt (model grid step = 50 m.) selected from the larger Alexandria Sea (model grid step = 1.25 Km), which in turn was chosen from the Egyptian Mediterranean coastal area (model grid step = 12.5 km). The sensitivity of the model simulations to both physical and biological main factors of the studied areas is tested. Both climatic conditions and land sources effects are considered among the model forcing factors. The resultant simulations are compared with the actual measured values of the parameters. The model sensitivity test results are discussed in the context of the model's capabilities and limitations, and with reference to the available knowledge of the ecosystems of the study areas.

Introduction

Management of coastal areas represents the key issue in the natural marine resources conservation policies. (Roberts and Polunin 1993; Dayton et al. 1995; Salomon et al. 2002). Indeed, sustainable management of coastal resources is found to be in urgent need of concrete information concerning the response of nature to both natural and man-made changes in the environmental forcing factors and loading (Pitcher and Pauly 1998; Tamsalu 1998). During the last few decades, numerical models have demonstrated their high capabilities in simulating and predicting such changes, especially due to the fast and accelerating progress in computer technology (Laevastu and Larkins 1981).

The necessity of coastal resources conservation polices or management polices or both is quite pronounced especially in developing countries, where, extensive urbanisation and industrial activities have caused increase in the coastal nutrient supply and consequently the development of eutrophication phenomena in specific areas. So, it becomes necessary to have a better understanding of the hydrodynamic and the ecosystem features of such areas. Indispensable for this are not only field surveys, but also the use of numerical models as a powerful tool in evaluating measures to be taken for anticipating any impact on

the studied ecosystem (Taguchi et al. 2002). Following the comprehensive review of coastal marine ecosystem modelling published by Fransz et al. (1991) different efforts have been paid to improve the sensitivity and the complexity of aquatic ecosystem models based on certain concepts regarding the linkage between the hydrodynamic and biological sub-models. On the European level, the ERSEM (European Regional Seas Ecosystem Model) was developed by Baretta et al. (1995), which is similar to the first version of the FinEst (Finnish-Estonian) model applied in the Baltic sea (Ennet et al. 1989). The FinEst model has been also applied in the Mediterranean coastal water with a special attention to the Egyptian coastal area by Hamza et al. (1998).

In the present study, the area of the Egyptian coast selected for ecosystem modelling extends between longitudes 29°45′ N and 33°45′ E and comprises about 75% of the entire continental shelf of the Egyptian coast, to a water depth of about 350–400 m. The ecosystem parameters of the chosen area were measured during 1982–1986 by the Oceanography Department, Faculty of Science, Alexandria University, Egypt, financed by a US Aid Project. Diverse environmental parameters covering physical, chemical, biological and geochemical aspects were seasonally measured along 10–12 transects, each with 25–30 sampling stations (Hamza 1995). The parametric data were earlier utilised in an ecosystem Fin-Est model. However, the application of the data was limited to the correlation of the various parameters over the study area. In addition, preliminary modelling for winter conditions provided concordant simulated results for the algae bloom around a discharging estuary of the Rosetta branch of the River Nile. High nutrient concentrations were also predicted and an explanation for the winter bloom on the Egyptian Mediterranean coastal area was developed (Hamza et al. 1998).

The aim of the present contribution is to implement the 3D-coupled physical-biological model and its application on the Egyptian Mediterranean coastal area as a simulating and predictive operating tool. Specifically, the model is focussed on a small selected target area, and the resulting features of this area are compared with those of the surrounding region. For this purpose, a software program was developed allowing any target area to be interactively chosen from the computer monitor. After setting the grid step reducing factor the program automatically creates model input files for the target area. The target area chosen is the Eastern Harbour of Alexandria, Egypt, with grid step = 50 m. This harbour forms part of the larger Alexandria Sea (model grid step = 1.25 Km), which is itself a component of the Egyptian Mediterranean coast (model grid step = 12.5 km). A test was designed to explore the sensitivity of the model for certain physical and biological main parameters for the study areas.

Features of the study area

The Egyptian coastal area forms a distinct segment of the North African coast, as it incorporates the Nile Delta Region (NDR). The delta has formed from sediments transported during flooding of the Nile, which occurred annually until 1960's when the floodwaters were regulated by the construction of the Aswan High Dam. The appearance of winter algae blooms, in the years following freshwater flood regulation reinforces the unique character of this part of the coastline, in terms of its ecosystem behaviour (Dowidar, 1984, 1988). The winter algae bloom development along the Egyptian Mediterranean coast was attributed mainly to the high discharge of nutrient rich freshwater from land run-offs (Nile river included) during winter season (> 40% of annual total flow). That flow is contributes to both dilution of water salinity and increase of nutrients concentrations, consequently stimulating algae bloom development (Hamza et al. 1998). Such factors made the ecosystem features along the Egyptian coast unique among the other Mediterranean coastal areas since the Aswan High Dam construction until now.

The city of Alexandria extends along the Mediterranean coast, and supports a large population (about 4.5 million inhabitants), which doubles during summer vacation time. The city has the largest commercial harbour in Egypt, as well as several fishery harbours, among which the eastern harbour was also exploited as a site for the discharge of untreated sewage from the city until 1973. Thereafter, primary treated sewage was discharged in large volumes, due to the increase in the urban population.

The main hydrographic and ecosystem features of the different study areas used in the Fin-Est model implementation may be summarised as follows:

Table 1. Location and discharge water characteristics of the main land-runoffs and the winter season discharge percentages.

Sources	Location		Discharge	Winter	Salinity	Nutrient loads	
	Lon. deg.	Lat. deg.	km^3/y^1	%	ppt	N t^3/y^1	P t^3/y^1
Lake. Mariut	29.82	31.20	2.3	40	6	90.85	11.41
Lake Idku	30.20	31.33	0.4	40	4	16.16	2.03
River Nile	30.37	31.50	3.5	90	2	138.17	17.35
Lake Burullus	31.00	31.62	2.2	40	5	87.14	10.94
N.Delta drains	31.28	31.55	3.5	40	4	138.17	17.35
Lake Manzalah	31.48	31.46	5.2	40	5	205.44	25.80
TOTAL	–	–		–	–	676.37	84.88

Hydrographic features

The main topographic and hydrologic features characterising the Egyptian Mediterranean coastal area are:

1. a wide shelf area with shallow coastal depth. This is mainly a result of the deltaic sediment build-up since ancient times; and
2. a huge volume of freshwater is discharged along the studied coastal area, mainly from land-runoff. The freshwater is derived not only from the River Nile water, but also from agriculture and sewage water reaching those coastal lakes that are connected directly or indirectly to the Mediterranean coastal area.

A list of the land-runoff water sources and their locations is presented in Table 1. Discharge rates for each source show higher values during the winter season compared with other seasons. The main contributor to the winter disharge is the Nile flood (through the Rosetta branch), which represents up to 90% of its annual discharge.

The annual total load of nutrient salts from land sources, is estimated to be 676.4 tons $year^{-1}$ dissolved nitrogen and 84.9 tons $year^{-1}$ dissolved phosphorus. These loads are carried by 17.1 km^3 $year^{-1}$ of discharge water from various land-runoffs, giving an overall flow rate of 453 m^3 sec^{-1} (Table 1).

The measured physical, chemical, and biological parameters were plotted against sample geographical position for each station: water temperature, water-salinity, macronutrient (NO_3-N, NH_4-N, PO_4-P, SiO_2-Si), chlorophyll-a, Secchi-disc readings, light attenution coefficient, primary productivity, and zooplankton standing crop. Correlations between these parameters were investigated on seasonal basis, as mentioned above. The result is the outlining of homogenous fields showing the spatial seasonal distribution of each parameter over the studied areas (Hamza 1995). Although a significant reduction in the volume of discharged freshwater has been achieved during the last 5 years, it is very important to run this model based on existing historical data, so as to simulate the actual change in the ecosystem due to the reduction in the nutrient load. However, it is recognised that the reduction in discharged water is unlikely to have an immediate effect on the living biota, because the bottom sediments are capable of storing nutrients from previous high discharges loaded with both organic and inorganic materials.

Ecosystem features

The main features that characterize the ecosystem of the Egyptian Mediterranean coastal areas are:

1. A- seasonal variations in water salinity ahead of NDR, during the autumn and winter seasons. The water-salinity values are mostly lower (average surface-water salinity = 3.84%) than for the surrounding offshore area (average surface water salinity = 3.91%).
2. B- estimated N:P ratios have higher values during winter (N:P range = 45–60) compared with other seasons (N:P range = 5–15), indicating phosphorus as a limiting factoring in winter. In contrast, the western side of the NDR is nitrogen limited during the other seasons (Dowidar 1984).
3. C- Both algae biomass (chlorophyll-a), and zooplankton standing crop values have higher concentrations (averages = 4.5 mg m^{-3}, average = 3×10^3 Ind. m^{-3}, respectively) during the winter season

compared with the other seasons (range = 0.5–1.5 mg m^{-3}, range = 1–2 × 10^3 Ind. m^{-3}, respectively).

4. D- A marked algae bloom in winter is mainly localized around the NDR and extends eastward. It is also important to mention that, seasonal primary productivity distribution in this area have high values during the autumn and winter seasons (average = 6.0 and 3.25 mg C m^{-3}, respectively) compared with the other two seasons (range = 0.5–1.5 mg C m^{-3}).

The above features have been presented as evidence (Dowidar 1988), confirming the effects of the regulation of the Nile floodwaters by the High Aswan Dam. The effect of the nutrient-rich Nile water discharge is discernible until almost the end of winter, at which time a high algae biomass has developed, assisted by climatic conditions.

Eastern harbour

The Eastern Harbour is a shallow (average depth of 6 m), semi-closed basin, which is sheltered from the sea by an artificial water-break interrupted by two openings, El-Boughaz and El-Silsila, that provide communication between the harbour water and the waters of the Egyptian Mediterranean coast. The surface area of the harbour is estimated to be 2.53 × 10^6 m^2. The harbour has limited variation in its surface water salinity maintained by a daily discharge of about 0.25 × 10^6 m^3 of urban sewage through a single pipe close to the surface water level. This voluminous discharge has resulted in a high nutrient load, not only as a dissolved component, but also within the sediments, which may be considered as the renewable nutrient source for the harbour ecosystem, especially if the sewage discharge flow is cut. The existing high nutrients concentration in the water has led to an increase in eutrophication of the harbour ecosystem. Since, the eastern harbour is used as a fishery port, a considerable amount of oil and grease also find their way into the sediments. To remedy these problems restoration programmes have been designed for the harbour environment before attempting recovery of the archaeological monuments found in its basin and imbedded in its polluted sediments.

Model description

Basic equations

The hydrodynamic-ecological model used is based on the 3-D free-surface primitive equation system which is written in reference surface following σ (sigma) coordinates. The governing equations of the model are the horizontal momentum equations for velocity components u, v under Boussinesq approximation; the hydrostatic approximation of the equation for the vertical velocity w; the continuity equation for incompressible fluid; state equation; transport-diffusion equation for temperature T, salinity S and biochemical tracer C. In Cartesian σ coordinate system they have the following symmetrized form (Zalesny 1996; Zalesny and Tamsalu 2000).

$$\left[D\frac{d}{dt} - \tilde{\Lambda}\right]u - Dfv = -D\left[g\frac{\partial\zeta}{\partial x} + F_u\right]; \quad (1)$$

$$\left[D\frac{d}{dt} - \tilde{\Lambda}\right]v + Dfu = -D\left[g\frac{\partial\zeta}{\partial y} + F_v\right];$$

$$\frac{1}{\rho_0}\frac{\partial p}{\partial\sigma} = Db; \frac{\partial D}{\partial t} + \frac{\partial Du}{\partial x} + \frac{\partial Dv}{\partial y} + \frac{\partial\omega}{\partial\sigma} = 0; b = f(T,S);$$

$$\left[D\frac{d}{dt} - \tilde{\Lambda}\right]T = 0; \left[D\frac{d}{dt} - \tilde{\Lambda}\right]S = 0; \left[D\frac{d}{dt} - \tilde{\Lambda}\right]C = F^{Eco} \quad \text{Here} \quad F_u = -\left[\frac{1}{\rho_0}\frac{\partial p}{\partial x} + \frac{1}{2}\left(Z\frac{\partial b}{\partial x} - b\frac{\partial Z}{\partial x}\right)\right]; F_v = -\left[\frac{1}{\rho_0}\frac{\partial p}{\partial y} + \frac{1}{2}\left(Z\frac{\partial b}{\partial y} - b\frac{\partial Z}{\partial y}\right)\right];$$

$$D\frac{d\phi}{dt} = \frac{1}{2}\left[\left(\frac{\partial D\phi}{\partial t} + D\frac{\partial\phi}{\partial t}\right)\right] + \frac{1}{2}\left[\frac{\partial Du\phi}{\partial x} + Du\frac{\partial\phi}{\partial x} + \frac{\partial Dv\phi}{\partial y} + Dv\frac{\partial\phi}{\partial y} + \frac{\partial w\phi}{\partial\sigma} + w\frac{\partial\phi}{\partial\sigma}\right]$$

$$\tilde{\Lambda}\phi = \frac{\partial}{\partial\sigma D}\frac{\nu_\phi\partial\phi}{\partial\sigma} + \frac{\partial}{\partial x}\mu_\phi D\frac{\partial\phi}{\partial x} + \frac{\partial}{\partial y}\mu_\phi D\frac{\partial\phi}{\partial y}$$

$$\sigma = \frac{Z + \zeta(x,y,t)}{D(x,y,t)},$$

Z is the original downward vertical coordinate; $Z = D\sigma - \zeta$; $\zeta(x,y,t)$ and $D(x,y,t)$ are reference functions, for example $\zeta(x,y,t)$ may be a surface elevation and $D(x,y,t)$ a total thickness of fluid: $D = H + \zeta$, $H(x,y)$ is the bottom relief; f is the Coriolis parameter; ν_φ and μ_φ are vertical and horizontal turbulent diffusion coefficients respectively, F^{eco} describe biochemical processes.

For better description of the biological processes in the upper euphotic layer we use a double σ coordinate system dividing the marine basin into two parts with respect to the vertical, D_1 and D_2, and introducing two corresponding σ

$$\sigma_1 = \frac{z_1 + \zeta}{D_1}; \sigma_2 = \frac{z_2 + \zeta}{D_2}; D_1 = h + \zeta; D_2 = H - h. \tag{2}$$

Where $\boldsymbol{h}$ is the undisturbed thickness of the upper layer. For calculation of vertical turbulent mixing the Reynolds-averaged turbulent energy density equation is used (see Tamsalu, 1998; Ennet, Kuosa and Tamsalu, 2000) The corresponding boundary and initial conditions are added to the system (1). To solve Equations (1) with respect to time we use a splitting-up method with respect to physical processes (macro-level of splitting) and spatial coordinates (micro-level). We represent the operator of the system (1) as a sum of sub-operators and reduce the solution of the original problem with complicated operator A to that of number of problems with simpler operators A_{ij}:

$$A = \sum_{i=1}^{N} \left(\sum_{j=1}^{J} A_{ij} \right) \tag{3}$$

To do that we extract two macro-splitting steps which describe basic physical processes (1) transport-diffusion of momentum, temperature, salinity and biochemical tracers; adaption of velocity and density fields. To resolve 3D transport-diffusion equations effectively we use splitting with respect to separate coordinates x, y, σ. For spatial approximation of the Equations (1) we use the combination of A and C grids. For transport-diffusion equations, A grid is used, and for adaption of velocity and density fields, C grid is used.

The ecosystem model consists of the plankton community, inorganic nutrients, organic nutrients and detritus sub-models. Our planktonic community model is formed by four size classes of autotrophs (A_n) and heterotrophs (H_n) plus bacterioplankton (B). Size-dependent planktonic food-web structure allows to reduce the number of model coefficients because many of the reaction rates are expressed as functions of plankton mass. The number of chosen size-classes in the model (4 size classes for autotrophs and 5 size-classes of heterotrophs) enables to cover the entire spectrum of planktonic organisms in the aquatic ecosystem. This plankton community food web is expressed here by four triplets, each one formed by one heterotrophic predator-grazer, one phytoplankton and one zooplankton prey. In the last (fourth) triplet the zooplankton prey is to be replaced by bacterioplankton. While, in the first triplet predation by fish is significant as a controlling factor for mesozooplankton and is therefore excluded from the model (see Figure 1).

Following the general idea of Volterra (1932) we wrote the prey and predator plankton community equations in the following form (Tamsalu and Ennet 1995; Tamsalu 1998; Ennet et al. 2000).

$$\left[D\frac{d}{dt} - \tilde{\Lambda} \right] A_n = D[(Ca_n ga_n - Dam_n - Dar_n - Dae_n)A_n - Ch_n \times gh_n \times H_n \times A_n^2] - \omega_n \frac{\partial A_n}{\partial \sigma} \tag{4}$$

$$\left[D\frac{d}{dt} - \tilde{\Lambda} \right] H_n = D[(Ch_n \beta \times gh_n (A_n^2 + H_{n+1}^{n+1}) - Dhm_n - Dhr_n - Dhe_n)H_n - Ch_{n-1} \times gh_{n-1} \times H_{n-1} \times H_n^2]$$

$$\left[D\frac{d}{dt} - \tilde{\Lambda} \right] B = D[(Cbgb - Dbr - Dbe)B - Ch_N \times gh_N \times H_N \times B^2]$$

Here $n = 1,\ldots,N$ If $n = 1$ then $H_{n-1} = 0$ and if $n = N$ then $H_{n+1} = B$ Ca_n, Ch_n, Cb are maximum growth rate for autotrophs, heterotrophs and bacterioplankton respectively; ga_n, gh_n, gb are Michaelis-Menton kinetics functions for autotrophs, heterotrophs and bacterioplankton respectively; Dam_n, Dar_n, Dae_n are mortality, respiration and excretion rates for autotro-

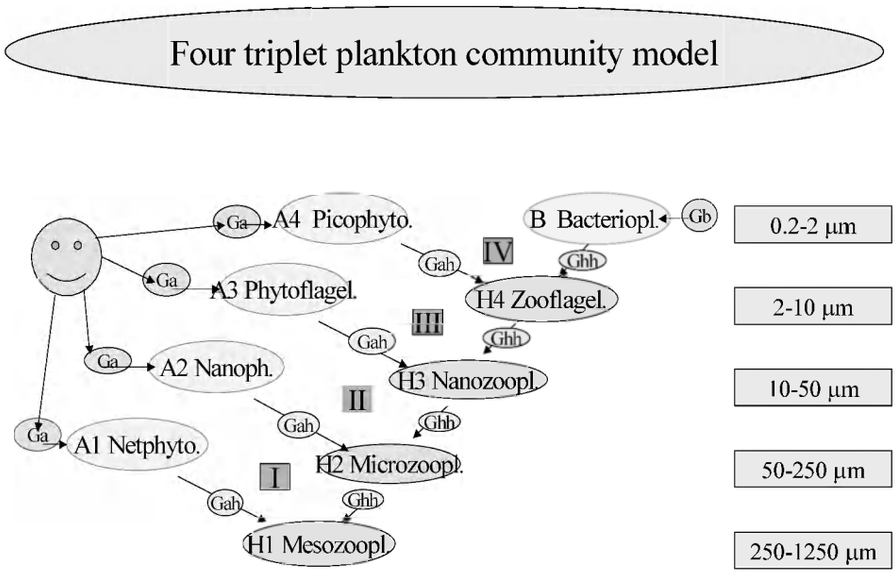

Figure 1. Four triplet plankton community food web.

phs, respectively; Dhm_n, Dhr_n, Dhe_n are mortality, respiration and excretion rates for heterotrophs, respectively; Dbr, Dbe are respiration and excretion rates for bacterioplankton, respectively; ω_n is the settling velocity, β is the efficiency coefficient. N is the numbers of autotrophs and heterotrophs in the plankton community system ($N = 4$). The energy flows to the plankton community comprises the uptake of dissolved inorganic nutrients by phytoplankton and is directed from the autotrophs toward heterotrophs through grazing; and dissolved organic and inorganic nutrients by bacterioplankton and is directed towards the larger size-groups of heterotrophs through predation. Energy is lost through mortality, respiration, exudation, excretion and sedimentation. For parameterisation of the biochemical reactions we use first-order (linear) kinetics relationships for mortality, respiration, exudation and excretion; the quasi-linear Michaeles-Menten growth kinetics for autotrophic and bacterioplankton uptake; and second-order (non-linear) kinetics for grazing and predation. Here the food consumption (uptake) functions are presented by a Michaelis-Menten expression for autotrophs (ga_n), bacterioplankton (gb) and heterotrophs (gh_n).

$$gh_n = f_{THn} \frac{1}{caz_n(A_n + H_{n+1}) + A_n^2 + H_{n+1}^n}$$

$$ga_n = f_{TA} \times f(I) \times \min\left(\frac{DIP}{cap_i + DIP}, \frac{DIN}{can_i + DIN}, \frac{DIC}{cac_i + DIC}\right)$$

$$gb = f_{TB} \times \min\left(\frac{DIP + DOP}{cap_i + DIP + DOP}, \frac{DIN + DON}{can_i + DIN + DON}, \frac{DOC}{cac_i + DOC}\right)$$

$$f(I) = \frac{I}{cai + I}$$

Here $I = PAR^* I_0 exp(-az)$ is the diffuse light, PAR is the photosynthetic available radiance (400–700 nm), I_0 is the global radiation on the water surface, $\boldsymbol{a}$ is the extinction coefficient, which is kept as a function of the plankton biomass and detritus. $DIP = PO_4$ is the inorganic phosphorus, $DIN = NH_4 + NO_3$ is the available inorganic nitrogen for algae uptake, $DIC = CO_2$ is the inorganic carbon. DOP, DON and DOC are dissolved organic phosphorus, nitrogen and carbon respectively. The influence of temperature is taken into account through a temperature limitation factor (f_{TA}, f_{TB}, f_{TH}); cap_n, can_n, cac_n, cai, are the half-saturation coefficients for autotrophic uptake and caz_n is the half-saturation coefficient for heterotroph growth.

The main problem in solving of the plankton community Equations (4) is the great number of the empirical coefficients, especially coefficients for maximum growth rate. Using the investigations published by Moloney and Field (1991) and Barenblatt (1996), Tamsalu (1998) the maximum growth rate, as with all other biochemical reactions needed in describing the plankton community, is dependent on plankton biomass:

Table 2. Model parameters.

Parameter	Value	Unit	Description
ca	6.0	$g^{1/4}d^{-1}$	Coefficient for autotrophs uptake
ch	6.0*ca	$g^{1/4}d^{-1}$	Coefficient for heterotrophs ingestion
dm	0.05	–	Proportionality coefficient for mortality
de	0.05	–	Proportionality coefficient for execudation or excretion
dr	0.025	–	Proportionality coefficient for respiration
cc	0.11	G/g	Carbon fraction in biota
	cp = cc/42	G/g	Phosphorus fraction in biota (calculated by using P:C ratio)
	cn = cp*7.2	G/g	Nitrogen fraction in biota (calculated by using N:P ratio)
cza	0.49	$g^{23/25}m^{-3}$	Half-saturation coefficient for ingestion
cca	0.0018	$g^{3/5}m^{-3}$	Half-saturation coefficient for carbon uptake
	cpa = cca/42	$g^{3/5}m^{-3}$	Half-saturation coefficient for nitrogen uptake (calculated by using P:C ratio)
	can = cpa*7.2	$g^{3/5}m^{-3}$	Half-saturation coefficient for nitrogen uptake (calculated by using P:N ratio)
Dd	0.05	d^{-1}	Maximum decay rate of particulate substance
dn_1	5.0	d^{-1}	Maximum nitrate nitrogen denitrification rate
dn_2	10.0	d^{-1}	Maximum nitrite nitrogen nitrification rate
dn_3	0.1	–	Maximum ammonium nitrogen nitrification rate
β	0.75	–	Efficiency coefficient
co_1	4.47	–	Oxygen consumption of nitrification
co_2	1.14	–	Oxygen consumption of denitrification
co_3	1.45	–	Oxygen consumption of detritus decay
co_4	1.80	–	Oxygen production of plankton growth and oxygen consumption of plankton respiration

$$\begin{aligned}\begin{Bmatrix} Ca_n \\ Ch_n \\ Cb \end{Bmatrix} &= \begin{Bmatrix} ca\times Ma_n^{-1/4} \\ ch\times Mh_n^{-1/4} \\ ca\times Mb^{-1/4} \end{Bmatrix}, \begin{Bmatrix} Dam_n \\ Dar_n \\ Dae_n \end{Bmatrix} \\ &= ca\begin{Bmatrix} dm \\ dr \\ de \end{Bmatrix} Ma_n^{-1/4}, \begin{Bmatrix} Dhm_n \\ Dhr_n \\ Dhe_n \end{Bmatrix} \\ &= ch\begin{Bmatrix} dm \\ dr \\ de \end{Bmatrix} Mh_n^{-1/4}, \begin{Bmatrix} Dbr \\ Dbe \end{Bmatrix} \\ &= ca\begin{Bmatrix} dr \\ de \end{Bmatrix} Mb^{-1/4} \end{aligned} \quad (5)$$

Following Moloney and Field (1991) the half-saturation coefficients are also mass-dependent functions

$$\begin{Bmatrix} cap_n \\ can_n \\ cac_n \end{Bmatrix} = \begin{Bmatrix} cpa \\ cna \\ cca \end{Bmatrix} Ma_n^{2/5} \quad (6)$$

$$caz_n = cza\times Ma_n^{2/25}$$

Here *ca,ch,dm,dr,de,cpa,cna,cca,cza* are universal coefficients; *Ma, Mh* and *Mb* are body mass of the autotrophs, heterotrophs and bacterioplankton respectively (see Table 2). By this parameterisation the number of fitting coefficients was decreased 5 times. The dead autotrophs and heterotrophs become dead organic matter-detritus (*Det*), which is sinking to the bottom and decomposed the inorganic nutrients (D_{det}).

$$\left[D\frac{d}{dt} - \tilde{\Lambda}\right] Det = D[dm\sum_{n=1}^{N}(Ca_n\times A_n + Ch_n\times H_n) - D_{det}\times Det] - w_{det}\frac{\partial Det}{\partial\sigma} \quad (7)$$

D_{det} = *dd*cgtd**(1 – *exp*(–0.75**O* $_2$ + 0.14)), (see Kinnunen and Nyholm (1982)) Where *dd* is the max-

imum detritus decay, *cgtd* is the temperature factor and w_{det} is the detritus sinking velocity.

The model contains two compounds of phosphorus: i.e., phosphate phosphorus (PO_4) and dissolved organic phosphorus (*DOP*). The nitrogen block consists of nitrate nitrogen (NO_3), nitrite nitrogen (NO_2), ammonium nitrogen (NH_4) and dissolved organic nitrogen (*DON*). Besides the phosphorus and nitrogen the model contains two compounds of carbon, i.e., carbon dioxide (CO_2) and dissolved organic carbon (*DOC*). The available for autotrophs growth dissolved inorganic phosphorus ($DIP = PO_4$), nitrogen ($DIN = NO_3 + NH_4$) and dissolved inorganic carbon ($DIC = CO_2$) will be calculated as follows:

$$\left[D\frac{d}{dt} - \tilde{\Lambda}\right]\begin{pmatrix} PO_4 \\ NO_3 \\ NO_2 \\ NH_4 \\ CO_2 \end{pmatrix} = D\begin{pmatrix} cp \\ cn \\ cn \\ cn \\ cc \end{pmatrix} \times \left[-\begin{pmatrix} 1 \\ \gamma n_1 \\ 0 \\ 1-\gamma n_1 \\ 1 \end{pmatrix} \sum_{n=1}^{N} Ga_n - \begin{pmatrix} 1-\gamma p \\ \gamma n_2 \\ 0 \\ \gamma n_3 \\ 0 \end{pmatrix} Gb + \begin{pmatrix} \varepsilon_1 \\ 0 \\ 0 \\ \varepsilon_1 \\ \varepsilon_1 \end{pmatrix} D_{\det} \times Det + \begin{pmatrix} 0 \\ 0 \\ 0 \\ 0 \\ 1 \end{pmatrix} \left(\sum_{n=1}^{N} Dr_n + Dr_b\right) \right] + D\begin{pmatrix} 0 \\ Dn_2 - Dn_1 \\ Dn_3 - Dn_2 \\ Dn_3 \\ 0 \end{pmatrix} \tag{8}$$

$$Ga_n = Ca_n \times ga_n \times A_n; Gb = Cb \times gb \times B; Dr_n = Dar_n \times A_n + Dhr_n \times H_n; Dr_b = Dbr \times B$$

cp, *cn* and *cc* are phosphorus, nitrogen and carbon fraction in biota respectively, ϵ_1 is the proportionality coefficient. *Dn1* is the nitrate nitrogen denitrification, *Dn2* and *Dn3* are nitrite nitrogen and ammonium nitrogen nitrification, respectively.

$Dn_1 = dn_1 * cgtn * exp(-1.2 * O_2)$; $*NO_3$; (see Kinnunen and Nyholm 1982)

$Dn_2 = dn_2 * cgtn * (1 - exp(-1.5 * O_2)) * NO_2$; (see Kinnunen and Nyholm 1982)

$Dn_3 = dn_3 * cgtn * (1 - exp(-1.5 * O_2)) * NH_4$. (see Kinnunen and Nyholm 1982). dn_1, dn_2, dn_3 are empirical coefficients and *cgtn* is the temperature factor. The *DOP*, *DON* and *DOC*, which are used by bacterioplankton will be calculated by the following equations:

$$\left[D\frac{d}{dt} - \tilde{\Lambda}\right]\begin{pmatrix} DOP \\ DON \\ DOC \end{pmatrix} = D\begin{pmatrix} cp \\ cn \\ cc \end{pmatrix} \times \left[-\begin{pmatrix} \gamma p \\ \gamma n_4 \\ 1 \end{pmatrix} Gb + (1-\beta) \sum_{n=1}^{N} Gh_n + \sum_{n=1}^{N} De_n + De_b + \begin{pmatrix} 1-\varepsilon_1 \\ 1-\varepsilon_1 \\ 1-\varepsilon_1 \end{pmatrix} D_{\det} \times Det \right] \tag{9}$$

$$Gh_n = Ch_n \times gh_n \times (A_n^2 + H_n^2); De_n = Dae_n \times A_n + Dhe_n \times H_n; De_b = Dbe \times B$$

$$\gamma p = DOP/(DOP + PO_4); \gamma n_1 = NO_3/(NO_3 + NH_4);$$

$$\gamma n_2 = NO_3/(NO_3 + NH_4 + DON); \gamma n_3 = NH_4/(NO_3 + NH_4 + DON);$$

$$\gamma n_4 = 1 - \gamma n_2 - \gamma n_3$$

The dissolved oxygen will be calculated as follows

$$\left[D\frac{d}{dt}-\tilde{\Lambda}\right]O_2 = D\left[\begin{array}{l} co4\sum_{n=1}^{N+1}(Ga_n - Dar_n - Dhr_n - Gb) - \\ -co3\times D_{\text{det}} - co2\times Dn_2 - co1\times Dn_3 \end{array}\right] \tag{10}$$

Here co_1, co_2, co_3, co_4 are empirical coefficients. The bottom sediments components are organic matter (Det_s), phosphorus (PO_{4S}) and nitrogen (NO_{3S}, NO_{2S}, NH_{4S}) compounds and oxygen (O_{2S}). They are described as follows:

$$\left((1+p_\phi)\frac{\partial}{\partial t}+\begin{pmatrix} w_d \\ 0 \\ 0 \\ 0 \\ 0 \end{pmatrix}\frac{\partial}{\partial z}-\begin{pmatrix} \nu_D \\ \nu_P \\ \nu_{N1} \\ \nu_{N2} \\ \nu_{N3} \\ \nu_O \end{pmatrix}\frac{\partial^2}{\partial z^2}\right)\begin{Bmatrix} Det_S \\ PO_{4S} \\ NO_{3S} \\ NO_{2S} \\ NH_{4S} \\ O_{2S} \end{Bmatrix} = \begin{Bmatrix} -D_{\text{det}S} \\ cp\times D_{\text{det}S} \\ Dn_{2S} - Dn_{1S} \\ Dn_{3S} - Dn_{2S} \\ cn\times D_{\text{det}S} - Dn_{3S} \\ -co3\times D_{\text{det}S} - co2\times Dn_{2S} - co1\times Dn_{3S} \end{Bmatrix} \tag{11}$$

$D_{detS} = dd*cgtd*(1 - exp(-0.75*O_{2S} + 0.14))*Det_S$ $Dn_{1S} = dn_1*cgtn* exp(- 1.2*O_{2S})$; $*NO_{3S}$; $Dn_{2S} = dn_2*cgtn*(1 - exp(- 1.5*O_{2S}))*NO_{2S}$; $Dn_{3S} = dn_3*cgtn*(1 - exp(- 1.5*O_{2S}))*NH_{4S}$. Where w_d is the sediment accumulation velocity, ν_φ are the diffusion coefficients, p_φ are the dimensionless distribution coefficients defined as the proportion between the concentration of the adsorbed and dissolved constituent, respectively (Ruardij and Van Raaphorst 1995). On the surface of the bottom sediments $O_{2S} \equiv 0$ and for other components $\partial\varphi/\partial z = 0$

Linking of models with different grid resolutions

Continental shelf areas are well known for their ecological, economical and scenic values. Wise use of the marine coastal zones must particularly take account of the ecological aspects. For effective management of coastal zones, characterisation of trends taking place in the aquatic environment is necessary. The only way to simultaneously analyse the physical, chemical and biological processes, for predicting the outcomes of different scenarios, is to use mathematical modelling. To apply the model to local marine coastal zones, it is necessary to use small grid steps, perhaps less than 100 m. However, with such small grid steps, it is technically impossible to include the effects of the surrounding marine areas that will have significant impact on the local processes in the study area.

Thus one of the more complicated problems in coastal area modelling is the handling of open boundaries and initial conditions (Aksnes and Lie 1990). Setting of open boundary conditions and initial conditions has significant influence on the results of both the hydrodynamic and ecosystem model calculations. One solution might be the coupling of the models. In this case we first calculate results for a larger area where the open boundaries are shifted relatively far out to sea. Then we run the model for some smaller area (zoom area) within the latter larger area and obtain the open boundary from previous results.

Much model input data is needed in applying the program to specific zoom areas. For this purpose we have adapted software to allow the operator to choose the zoom area interactively from the screen, set the grid step reducing factor, then run the program to create the following input files:

- Bottom relief data. Due to grid step reducing, the zoom version has new grid points, different to those of the main version, for which depths will be interpolated from the main version data.
- Meteorological data. On the basis of longitude/latitude coordinates the new meteorological input data files will be created.
- Rivers and pollution load data. River and pollution data relevant to the zoom area will be selected from the main version. The river and load zoom grid points will also be calculated.

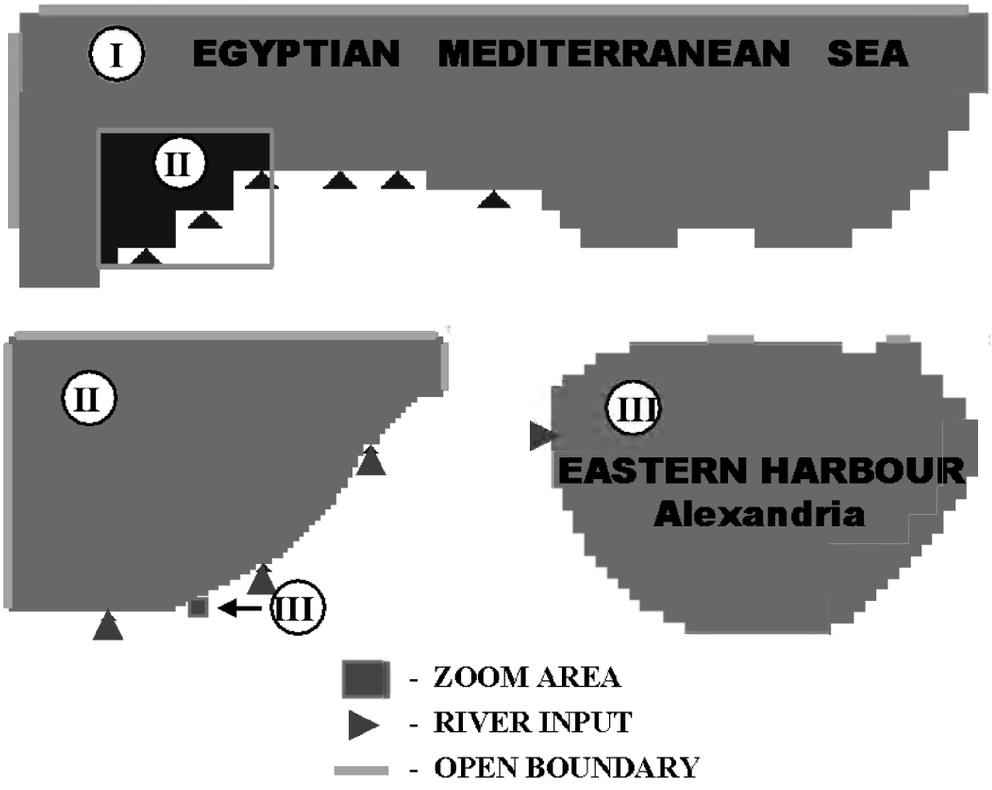

Figure 2. The model calculation areas in the Egyptian Coast (I- Egyptian Mediterranean Sea, II- Alexandria Sea, III- Eastern harbour-Alexandria).

- Open boundary data. The zoom version open boundary points will be connected to main version calculation points by comparing the main version grid sea/land points and zoom version grid sea/land points.
- Initial data. If the zoom version calculations start later than main version, then zoom version initial data will be read and interpolated from main version results.

The program was assigned to calculate results for small areas wherein the initial and open boundary conditions were derived from the analytical results for larger areas. The model simulations were performed on three scales for the following areas (Figure 2): I – the whole Egyptian Mediterranean Sea, II – Alexandrian sea area and III – Eastern Harbour area in Alexandria.

First the entire Egyptian Mediterranean Sea area was considered and these results were used to define open boundary conditions for the Alexandrian sea calculations. Finally, a small area, Eastern Harbour of Alexandria, was considered, with the open boundary conditions being obtained from the results of the Alexandrian sea calculations. All these calculations made use of year 1997 meteorological data from the NOAA CIRES Climate Diagnostics Center, Colorado.

A brief description of the method used to calculate the open boundary conditions for the small calculation area is presented below:

- *The first step – calculations for the entire Egyptian Mediterranean Sea*. The calculations relate to an area bounded by longitudes 29.0° E to 34.8° E and latitudes 30.7° N to 32.3° N. The model grid size was 52 × 16 in the East and North directions, respectively, with a grid step of 12.5 km. Twelve vertically stacked layers (6 in the upper layer and 6 in the lower layer) were used in the calculations. The number of model calculation points in each horizontal layer was 513. For the open boundaries (10 calculation points from East and 43 calculation points from North in one layer) the value constants for

model variables were set. Calculations were run modelling one year with 10 minute time steps; the model variables were stored for each 6 hours.

- *The second step – calculations of the Alexandrian Sea area with open boundary conditions derived from the entire Egyptian Mediterranean Sea calculations.* For the Alexandrian Sea the model area was selected from the first-step calculations grid as shown in Figure 2. Grid size was 83 × 53 in the East and North directions, respectively. 12 vertically stacked layers were used. The number of model calculation points in each horizontal layer was 3194. The grid step, at 1.25 km, was chosen to be one tenth of the first-step grid. During calculations of the open boundaries (49 calculation points from the East, 81 calculation points from the North and 9 calculation points from the West in each layer) the model variable values were input for each layer, every 6 hours, from the previous entire Egyptian Mediterranean Sea calculations results. The model period was two months.
- *The third step – calculations for the Eastern Harbour in Alexandria with open boundary conditions derived from the Alexandrian Sea calculations.* The Eastern Harbour of Alexandria was chosen as an example of a small study area. This time a 50-m horizontal grid step was used. The grid size was 40 × 28 in the East and North directions, respectively. 12 vertically stacked layers were again used. The number of model calculation points in each horizontal layer was 800.

The area considered was so small compared with the Alexandrian Sea calculation area that only one of the Alexandrian area calculation points was relevant to use for Eastern Harbour open boundary (6 points from North). The simulation period was 25 days. During calculations these six open boundary points were linked to Alexandrian Sea calculation results. In the calculations of the Eastern Harbour the baroclinic part of the circulations was not used ($F_u \equiv F_v \equiv 0$ in Equation (1)), because the hydrostatic approximation does not work for this small grid.

Numerical results and discussion

Egyptian Mediterranean Sea

Initially the calculations were carried out for the entire Egyptian Mediterranean Sea. To minimise the unduly large influence of open boundaries for the coastal zone, the open boundary from North was set more than 100 km from the coast. Comparing the calculated distribution of temperature, salinity, nutrients and phytoflagellates for the middle of January the coastal zones with off shore zones the remarkable influence of the river Nile becomes quite evident (Figure 3), along with other point sources of salinity and nutrient concentrations. The three cross-sections of the salinity profiles (Figure 4), extend c. 30 km from the shore and to depths of 200 m. The calculated PO_4, NH_4, phytoplankton and zooplankton concentrations during January–March (Figure 5) are compared with actual measured data (Hamza 1995). This period was chosen because the plankton growth actively during winter in Egyptian Mediterranean Sea. The measured data represent the monthly mean concentrations and they can be regarded as representative values. To avoid the overwhelming effects of nearby nutrient sources on concentrations, the comparison point was chosen far from shore. The calculated PO_4 values are quite similar to the measured values, while calculated NH_4 values are consistently lower than measured ones. The reason for the latter is that in this period the calculated phytoplankton concentration was somewhat higher than normal, leading to more intensive use of NH_4, because of the nitrogen limitation conditions (Morcos and El-Rayis 1973). Also the comparatively higher calculated zooplankton concentration is caused by higher phytoplankton growth. The phytoplankton calculation in Figure 5 represents the sum of net-phytoplankton, nanophytoplankton, phytoflagellates and picophytoplankton. The calculated zooplankton is the sum of mesozooplankton, microzooplankton, nanozooplankton and zooflagellates. Nutrients uptake by bacterioplankton system is: 1. of dissolved inorganic nutrients and 2. of the dissolved organic nutrients uptake by bacterioplankton. The high zooplankton concentration (Figure 5) could be explained by the energy flow from bacterioplankton.

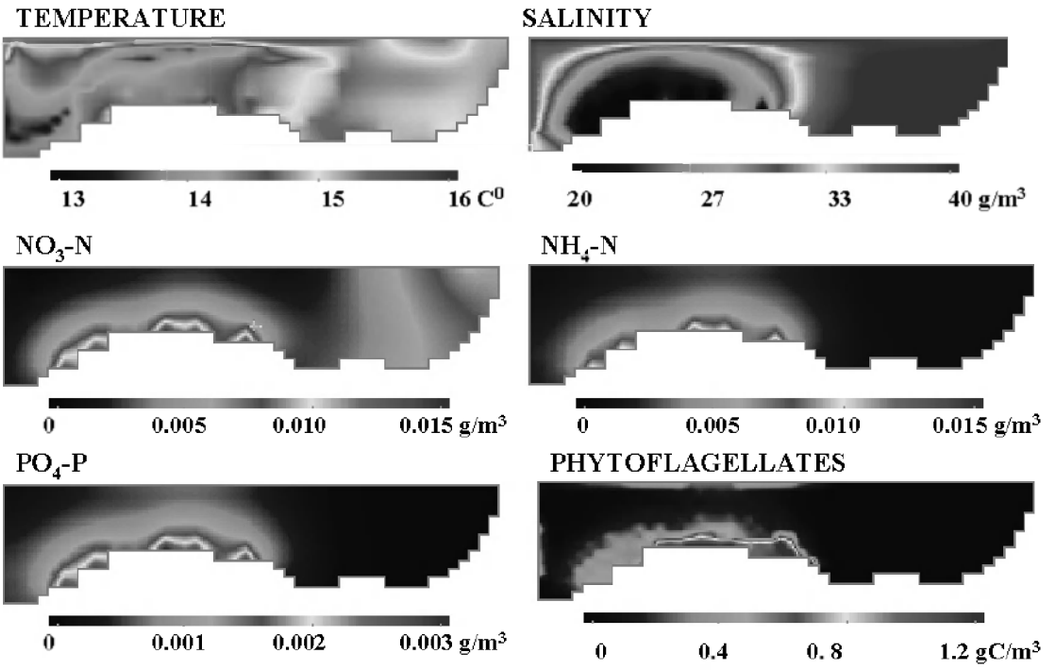

Figure 3. Distribution of calculated ecosystem parameters along the Egyptian Mediterranean coastal area.

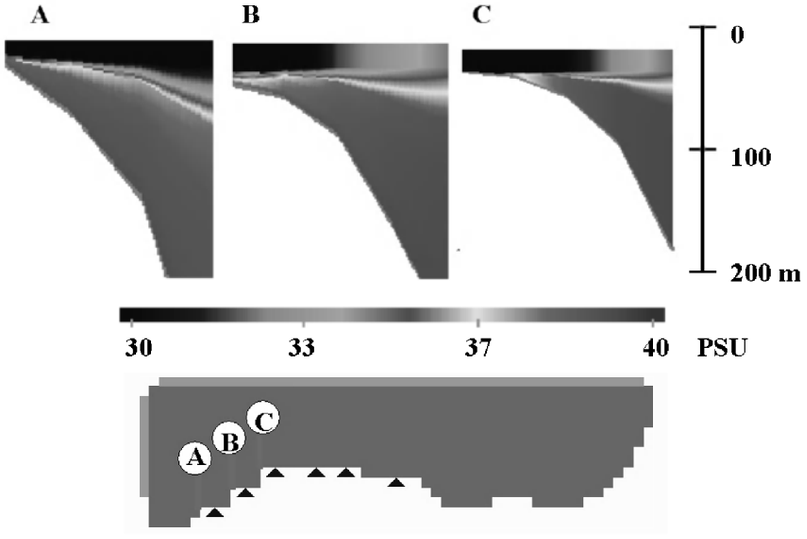

Figure 4. Calculated vertical distribution of salinity in three selected cross-sections.

Mediterranean Sea surrounding Alexandria

In these calculations the open boundary values were adopted from the entire Egyptian Mediterranean Sea calculation results. Thus the open boundary point model variables were made to vary with time, in accordance with values for these points calculated for the entire Mediterranean Sea. The calculated phytoplankton and zooplankton concentrations are presented in three near-shore points (Figure 6) which include: 1 – close to Lake Mariut inflow, 2 – close to Alexandria, 3 – near the Nile inflow.

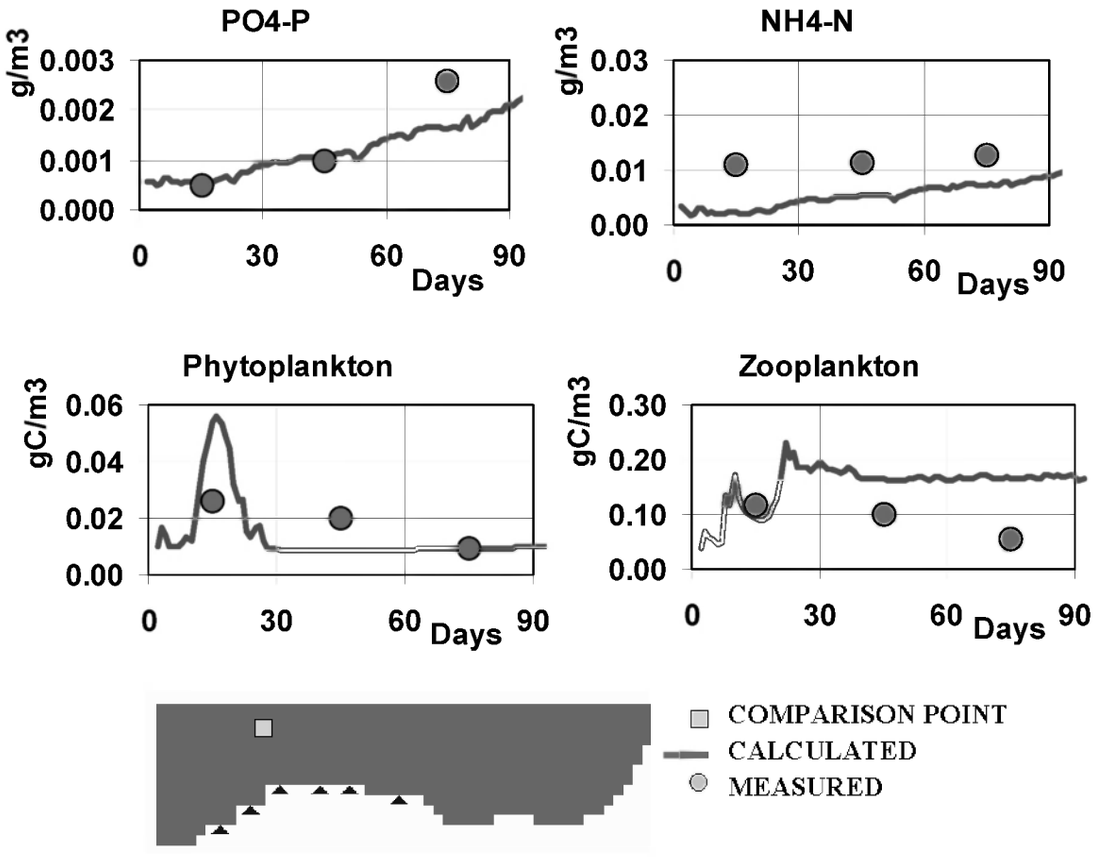

Figure 5. Comparison between measured and calculated values of nutrients and plankton concentrations at a selected grid step.

The plankton growth at these inshore points is strongly influenced by nutrient sources. Compared with offshore areas (Figure 5) the growth rates in the inshore areas are significantly higher. The calculated concentrations for different plankton size classes indicate that the phytoplankton dominated by the small size classes. The phytoplankton biomass is mainly comprised of phytoflagellates and picophytoplankton. The reason here is that their ability to utilizing available nutrients and to fit with existing environmental conditions are much higher compared with netphytoplankton and nanophytoplankton, and so they can use the nutrients more efficiently.

Eastern harbour of Alexandria

For this most detailed scale model, calculations of the phytoplankton concentrations were made for a 25-day model period during January. Two points representing the nearby discharging sewage site (point no. 1), and on the opposite side of the discharging sewage pipe (point no. 2), were selected for comparison. The results (Figure 7), indicate a high plankton concentration toward the nearby sewage site, where picoplankton represent the dominant group of the phytoplankton community. Such patterns may change seasonally because of changes in physical parameters.

On the other hand, the pattern of nutrient (PO_4-P, NO_3-N, NH_4-N) concentrations during January is indicative of the high nutrients load that is discharging almost into the harbour basin due to heavy rains drainage through sewage net-system (Figure 8). This load could be diluted, utilised, deposited and also diffused into the open water through the El-Boughaz harbour opening. Time series simulations of the calculated nutrients have also indicated slightly higher concentrations at the discharging point site as compared with the selected opposite site (Figure 9).

The results obtained from this modelling exercise have shown the success of the developed zoom op-

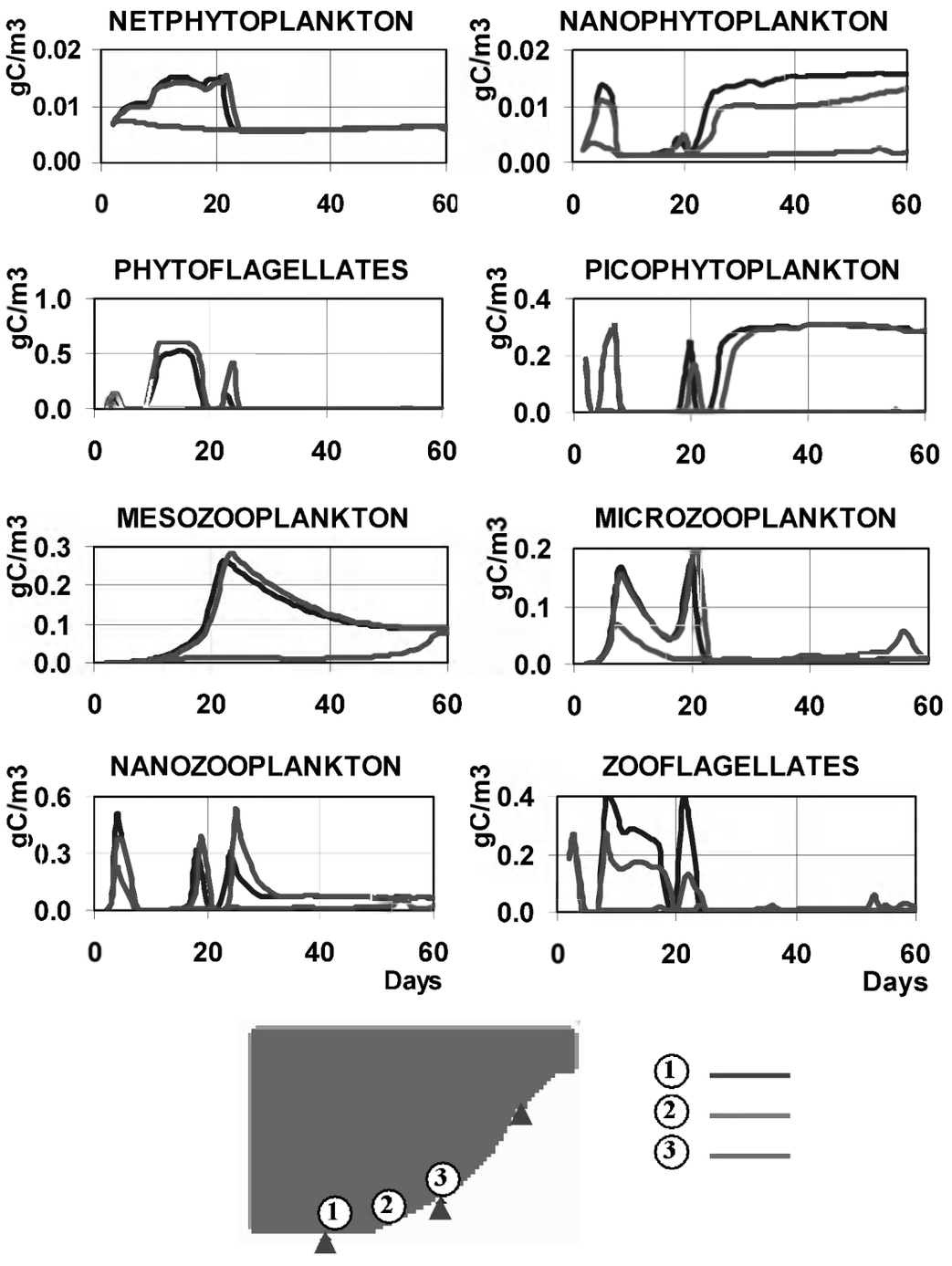

Figure 6. Calculated plankton concentrations at selected three points close to Alexandria coast during winter.

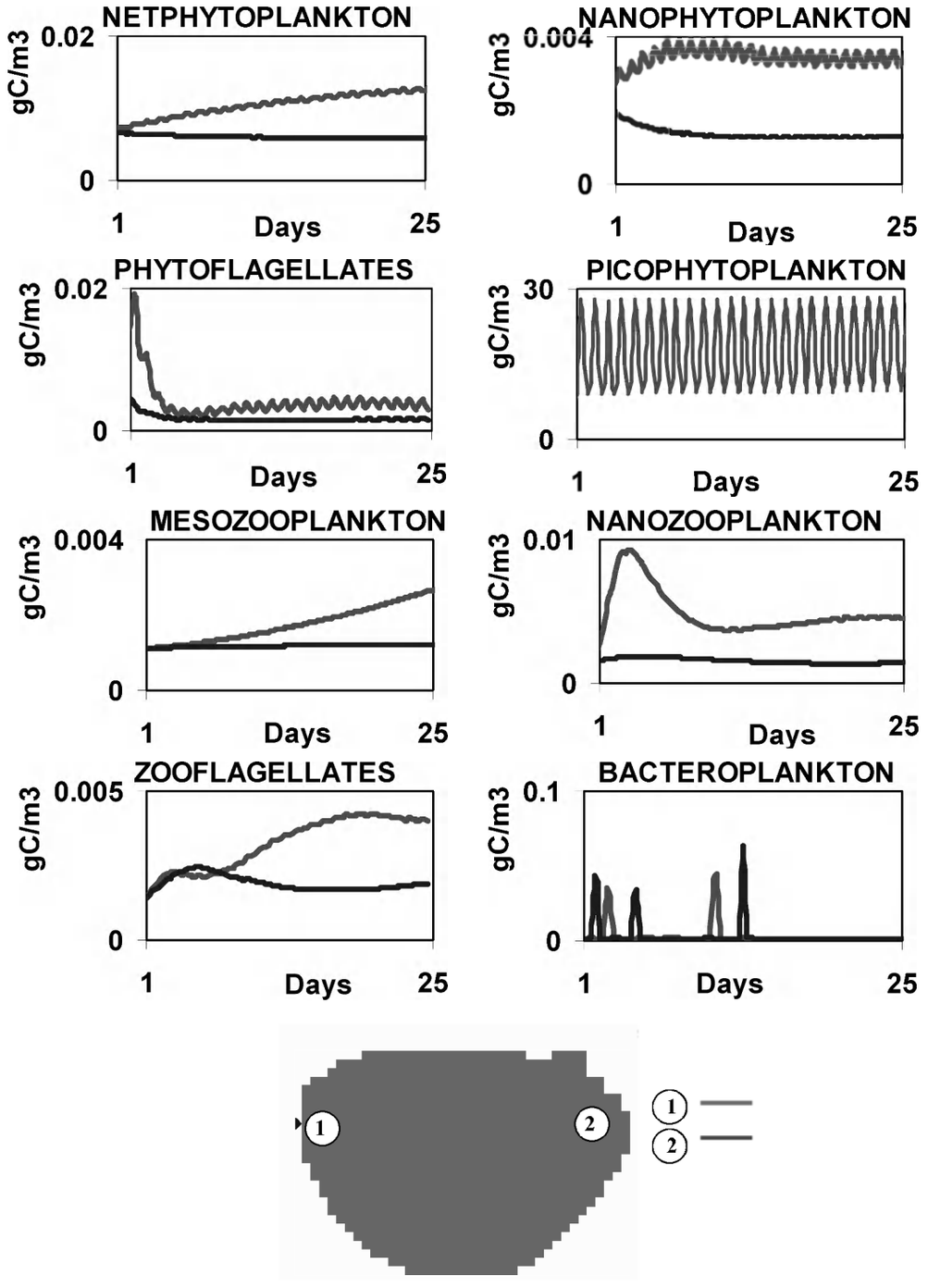

Figure 7. Calculated plankton concentrations at the sewage discharging point (1) and the opposite point (2) in the Eastern harbour.

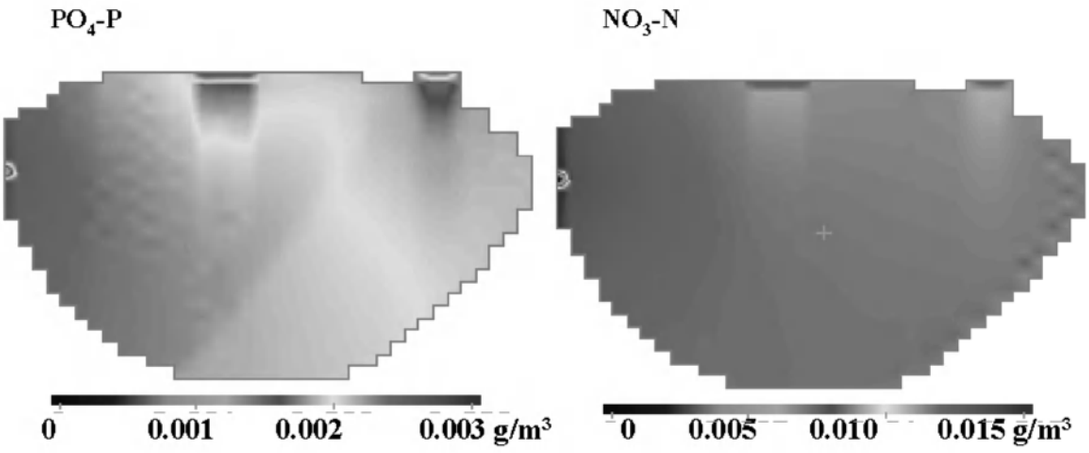

Figure 8. Distribution of PO_4 and NO_3 concentrations in the Eastern harbour during winter.

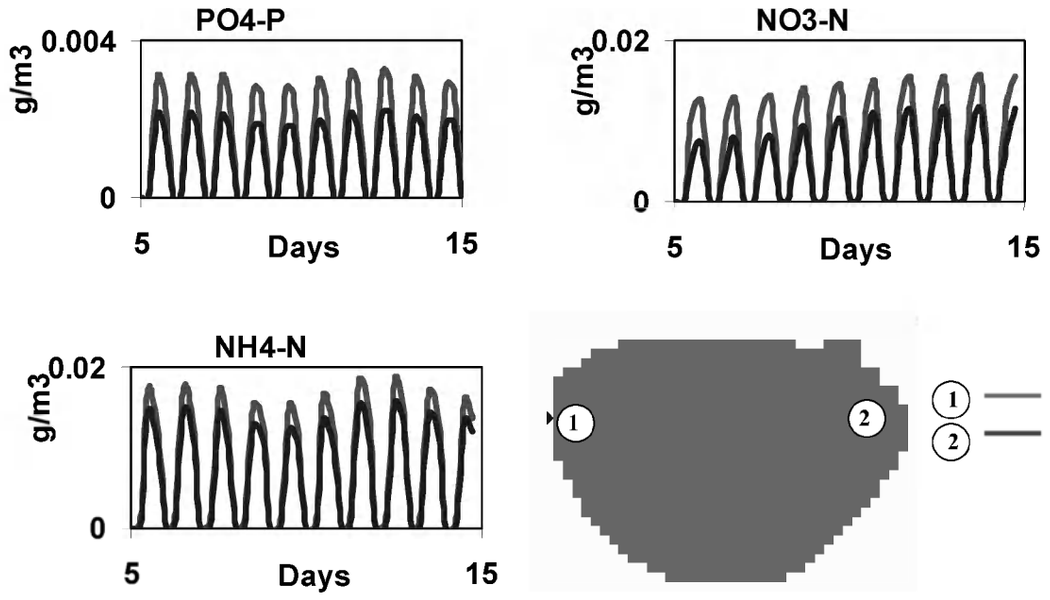

Figure 9. Comparison between the concentrations of nutrient salts at the sewage discharging point (1) and the opposite point (2) in the Eastern harbour.

tion in the coupled 3D physical-biological model. Indeed, it proves its reliability in the calculation of nutrients and concentrations by providing similar results to the measured values in the Eastern harbour (Abdel-Moati 1996).

Conclusions

The most important steps for developing a model that explains local features in the coastal ecosystem of the Egyptian Mediterranean, using zoom techniques, are summarised below:

One of the more complicated problems in coastal area modelling is the handling of open boundaries and initial conditions. The chosen open boundary conditions and initial conditions have significant influence on both the hydrodynamic and ecosystem model results. The solution employed here is to couple the models in such a way that the open boundary values of the smaller scale model are obtained from the previous larger scale model results.

In selecting a particular zoom area it is necessary to collect a lot of model input data. For this purpose software was developed which allows for automatic creation of input data files for the chosen zoom area. In the Egyptian Mediterranean coastal area, especially near to the shore, phytoplankton communities are dominated by small size classes of phytoplankton – phytoflagellates and picophytoplankton. The reason may be that their growth rates are much higher compared with netphytoplankton and nanophytoplankton, due to their more efficient use of nutrients. In addition, the continuous discharging of land source effluents with high concentartions of suspended matter and the resulting instability in the water column, and the intensive grazing by fish fry and zooplankton on the larger phytoplankton size classes, could favour the small size class dominance.

Using the mass-dependent parameterization for biochemical reactions (Moloney and Field 1991) the number of fitting parameters was decreased from 30 to 6. As a result, the plankton community equation system could be solved in a mathematically correct form. While a simple plankton community submodel needs very complicated parametrizations as well as calibrated coefficients, depending on environmental conditions, the mass-dependent parametrization for a size-dependent plankton community food web is simple and has a universal character. In our dataset the phytolankton community was taxonomicaly ranked according to their size classes.

It is unlikely that the existing plan to reducing the freshwater discharge from the Nile River will significantly affect the nutrients concentration in this area, especially because large quantities of primary treated sewage are still being discharged. However, the expected increase in the average water salinity may occur, if the freshwater discharge is reduced. This in turn may affect the community structure of the living biota – an outcome that can have both positive and negative impact on the fish productivity in this area. For this reason 3D coupled physical-biological model application with updated information could play a significant role in predicting and simulating the effect of the changing conditions.

Last, this work is the first step in the creation of an operational aquatic ecosystem model for coastal environment management and forecasting man-made impact on the ecological features of the studied area.

Acknowledgements

The present study was financially supported by EU-MAST-III CT-98 program through the MFSPP (Mediterranean Forecasting System Pilot Project). The first author of this work represents the Egyptian partner of the MFSPP under a sub-contractor with ISAO-CNR, Italy as UALEX-FS-DES (P-28). The authors would like to thank the W.L. Center in Erice, Italy and the Estonian Marine Institute and the Oceanography Dept., Alexandria University, Egypt for their help in initiating, encouraging, supporting and hosting the modeling work throughout the MFSP-Project. The data sets used in this work were collected from several Egyptian participants in the US-funded project, including the first author, for studying the primary productivity in the Southeastern Mediterranean. To all the contributors we are grateful. Finally, we would like to thank the reviewers for their critical reviews, which greatly helped us to improve the latest version of the manuscript.

References

Abdel-Moati M.A.R. 1996. Eutrophication in the coastal waters of Alexandria following the increase in phosphorus load. Fresenius Envir. Bull. 5: 172–177.

Aksnes D.L. and Lie U. 1990. A coupled physical-biological pelagic model of a shallow sill fjord. Estuar. Coast. Shelf. Sci. 31: 456–486.

Barenblatt G.I. 1996. Scalling, Self-Similarity, and Intermediate Asymptotics. Cambridge University Press, United Kingtom, 386 p.

Baretta J., Ebenhon W. and Ruardij P. 1995. The European Regional Seas Ecosystem Model, a complex marine ecosystem model. Netherland Journal of Sea Research 8: 233–246.

Dayton P.K., Thrush S.F., Agardy M.T. and Hofman R.J. 1995. Environmental effect of marine fishing. Aquat. Conserv. Mar. Freshwater Ecosyst. 5: 205–232.

Dowidar N.M. 1984. Phytoplankton biomass and primary productivity of the Southeastern Mediterranean. Deep Sea Research 31: 983–1000.

Dowidar N.M. 1988. Productivity of the South-eastern Mediterranean. In: El-Sabh M.I. and Murty T.S. (eds), Natural and Man-Made Hazards. pp. 477–498.

Ennet P., Kinnunen K. and Tamsalu R. 1989. Ecosystem Model FINEST. Valgus, Tallinn, 89p.

Ennet P., Kuosa H. and Tamsalu R. 2000. The influence of upwelling and entrainment on algal bloom in the Baltic Sea. Journal of Marine Systems 25: 359–367.

Fransz H., Moammerts J. and Radach G. 1991. Ecological modelling of the North Sea. Netherlands Journal of Sea Research 28: 67–140.

Hamza W. 1995. Protection of Coastal Marine Environment in the Southern Mediterranean: Numerical Modelling application on

the Egyptian Coastal area (FINEST Model). Report. ICSC-World Laboratory, Land-3 Project. Erice, Italy, Lausanne-Switzerland 60 pp.

Hamza W., Ennet P. and Tamsalu R. 1998. The ecosystem calculation for the Egyptian part of the Mediterranean. In: Tamsalu R. (ed.), The Coupled 3D Hydrodynamic and Ecosystem Model FINEST. *MERI.* Vol. 35., pp. 143–148.

Kinnunen K. and Nyholm B. 1982. Water quality modelling of Finnish water bodies. Publ. Water Res. Inst. 46: 3–99.

Laevastu T. and Larkins H. 1981. Marine Fisheries Ecosystem, its Quantitative Evaluation and Management. Fishing New Books Ltd., Farnham, Surrey, UK, 159p.

Moloney C. and Field J. 1991. The size-dependent dynamics of plankton food webs. I. A. Simulation model of carbon and nitrogen flows. J. Plank. Res. 13: 1003–1103.

Morcos S.A. and El-Rayis O.A. 1973. The levantine intermediate water, oxygen and nutrients off Alexandria. Thalassia Jogoslavica 9: 13–18.

Pitcher T.J. and Pauly D. 1998. Rebuilding ecosystems, not sustainability, as the proper goal of fishery management. In: Pitcher T.J., Hart P.J.B. and Pauly D. (eds), Reinventing Fisheries Management. Fish Fish. Ser. Vol. 23. Chapman and Hall, London, pp. 311–325.

Roberts C.M. and Polunin N.V.C. 1993. Marine reserves: simple solutions to managing complex fisheries? Ambio 22: 363–368.

Ruardij R. and Van Raaphorst W. 1995. Benthic nutrient regeneration in the ERSEM ecosystem model of the North Sea. Netherlands Journal of Sea Research 33: 453–483.

Salomon A.K., Walter N.P., McIlhagga C., Yung R.L. and Walters C. 2002. Modelling the trophic effects of marine protected areazoning policies: A case study. Aquatic Ecology 36: 85–95.

Taguchi K., Yamochi S., Oda K., Ishikawa K., Kido K. and Nakamura Y. 2002. Modelling population dynamics of the pelagic larval shrimp *Metapenaeus ensis* in the Osaka Bay estuary. Aquatic Ecology 36: 21–40.

Tamsalu R. 1998. Basic equations for a limited area. In: Tamsalu R. (ed.), The Coupled 3D Hydrodynamic and Ecosystem Model FINEST. *MERI.* Vol. 35., pp. 5–31.

Tamsalu R. and Ennet P. 1995. Ecosystem modelling in the Gulf of Finland. II. The aquatic ecosystem Model FINEST. Estuar. Coat. Shelf Sci. 41: 429–458.

Volterra V. 1932. Lecon sur la théorie mathématique de la lutte pour la vie. Gauthier-Villars.

Zalesny V.B. 1996. Numerical simulation and analysis of the sensitivity of large-scale ocean dynamics. Russ. J. Numer. Anal. Math. Modelling 11: 421–443.

Zalesny V.B. and Tamsalu R. 2000. Numerical analysis of the Marine dynamics. In: Proc. of Inter. Conf. “Numerical mathematics and mathematical modelling”. INM Ras, Moscow, pp. 110–124.